Heliyon 9 (2023) e19061

Contents lists available at ScienceDirect

Heliyon

journal homepage: www.cell.com/heliyon

Biosynthesis, characterization, and investigation of antimicrobial and cytotoxic activities of silver nanoparticles using *Solanum tuberosum* peel aqueous extract

Jiajun Xu [a,1], Mahmut Yıldıztekin [b,1], Dayong Han [a,*], Cumali Keskin [c,**], Ayşe Baran [d], Mehmet Fırat Baran [e], Aziz Eftekhari [f,l,***], Canan Aytuğ Ava [g], Sevgi İrtegün Kandemir [h], Deniz Bariş Cebe [i], Beşir Dağ [i], Aferin Beilerli [j], Rovshan Khalilov [k,l]

[a] *Department of Neurosurgery, The First Affiliated Hospital of Harbin Medical University, 23 Youzheng Str,Nangang District,Harbin,P.R.China, 150001*
[b] *Department of Herbal and Animal Production, Koycegiz Vocational School, Muğla Sıtkı Kocman University, Mugla, Turkey*
[c] *Department of Medical Services and Techniques, Vocational School of Health Services, Mardin Artuklu University, Mardin, Turkey*
[d] *Department of Biology, Graduate Education Institute, Mardin Artuklu University, Mardin, Turkey*
[e] *Department of Food Technology, Vocational School of Technical Sciences, Batman University, Batman, Turkey*
[f] *Department of Biochemistry, Faculty of Science, Ege University, Izmir, Turkey*
[g] *Dicle University Science and Technology Application and Research Center, Dicle University, Diyarbakır, Turkey*
[h] *Department of Medical Biology, Dicle University Central Research Laboratory, Faculty of Medicine, Dicle University, Diyarbakir, Turkey*
[i] *Department of Chemistry, Batman University, Batman, Turkey*
[j] *Department of Obstetrics and Gynecology, Tyumen State Medical University, 54 Odesskaya Street, 625023, Tyumen, Russia*
[k] *Department of Biophysics and Biochemistry, Baku State University, Baku, Azerbaijan*
[l] *Nanotechnology and Biochemical Toxicology (NBT) center, Azerbaijan State University of Economics (UNEC), Baku AZ1001, Azerbaijan*

ARTICLE INFO

Keywords:
Antimicrobial activity
Cytotoxic activity
Biogenic silver nanoparticles
Solanum tuberosum L.
Nanomedicine

ABSTRACT

Metallic nanoparticle biosynthesis is thought to offer opportunities for a wide range of biological uses. The green process of turning biological waste into utilizable products gaining attention due to its economical and eco-friendly approach in recent years. This study reported the ability of *Solanum tuberosum* (ST) peel extract to the green synthesis of non-toxic, stable, small-sized silver nanoparticles without any toxic reducing agent utilizing the phytochemical components present in its structure. UV–visible spectroscopy, X-ray diffraction analysis, Fourier transform infrared spectroscopy, flourier scanning electron microscopy, atomic force microscopy, transmission electron microscopy, and energy dispersive analysis X-ray confirmed the biosynthesis and characterization of silver nanoparticles. Also, dynamic light scattering and thermogravimetric analyses showed stable synthesized nanoparticles. The antibacterial activity of the biosynthesized

* Corresponding author.
** Corresponding author.
*** Corresponding author.
E-mail addresses: xujiajun@hrbmu.edu.cn (J. Xu), mahmutyildiztekin@mu.edu.tr (M. Yıldıztekin), hdybsn@163.com (D. Han), ckeskinoo@gmail.com (C. Keskin), ayse.gorgec43@gmail.com (A. Baran), mfiratbaran@gmail.com (M.F. Baran), eftekharia@tbzmed.ac.ir (A. Eftekhari), cananaytug@hotmail.com (C.A. Ava), irtegunsevgi@hotmail.com (S.İ. Kandemir), deniz.baris@batman.edu.tr (D.B. Cebe), besir.dag@hotmail.com (B. Dağ), abeilerli@mail.ru (A. Beilerli), hrovshan@hotmail.com (R. Khalilov).
[1] Equal contribution.

https://doi.org/10.1016/j.heliyon.2023.e19061
Received 25 June 2023; Received in revised form 7 August 2023; Accepted 9 August 2023
Available online 9 August 2023

silver nanoparticles was evaluated against four different bacterial strains, *Escherichia coli* (*E. coli*), *Pseudomonas aeruginosa* (*P. aeruginosa*), *Staphylococcus aureus* (*S. aureus*) *Bacillus subtilis* (*B. subtilis*), and a yeast, *Candida albicans* (*C. albicans*) using the minimum inhibitory concentration technique. The cytotoxic activities were determined against Human dermal fibroblast (HDF), glioblastoma (U118), colorectal adenocarcinoma (CaCo-2), and human ovarian (Skov-3) cell lines cancer cells using MTT test. The nanoparticle capping agents that could be involved in the reduction of silver ions to Ag NPs and their stabilization was identified using FTIR. Nanoparticles were spherical in shape and had a size ranging from 3.91 to 27.07 nm, showed crystalline nature, good stability (−31.3 mV), and the presence of capping agents. ST-Ag NPs significantly decreased the growth of bacterial strains after treatment. The in vitro analysis showed that the ST-Ag NPs demonstrated dose-dependent cytotoxicity against cell lines. Based on the data, it is feasible to infer that biogenic Ag NPs were capped with functional groups and demonstrated considerable potential as antibacterial and anticancer agents for biomedical and industrial applications.

1. Introduction

Nanotechnology is a young branch of research that deals with creating novel materials with special qualities at nanoscales between 1 and 100 nm for use in physics, biology, electronics, chemistry, agriculture, pharmacy, and other fields. It allows for the creation of novel nanomaterials, devices, and systems with unique functionality and qualities [1]. As a matter of fact, atoms near the surface of a nanostructure have fewer "neighboring" particles than do atoms in a bulky structure, which has an immediate effect on their atomic polarization and, in turn, the piezoelectric capabilities of nanomaterials (NMs). Furthermore, even in the absence of any externally applied pressures, surface stresses that induce significant strain on the atoms at the surface cause changes in the surface's polarization [2]. Environmentally friendly chemistry is provided as an alternate way that does not necessitate the use of environmentally hazardous procedures and materials. This option was created in reaction to the future catastrophic repercussions of the world and the limited time available to produce substantial answers [3].

Ag NPs may now be made using three different methods, including chemical, physical, and biological ones. Chemical methods, on the other hand, may include hazardous risks and generate dangerous byproducts. Additionally, the physical procedures have high energy and financial needs. The overwhelming requirement for an eco-friendly, low-energy, non-toxic, low-cost, and high-yield process significantly moved the attention to greener methods. Importantly, the limitations of physical and chemical processes are removed by the biological method of Ag NP synthesis. Numerous investigations have discovered that when compared to other conventional synthesis techniques that make use of potent elements such as inert gases, laser radiation, high pressure, high temperature, and so forth, biological synthesis techniques offer unique advantages. When opposed to chemical procedures, one drawback of biological approaches is that they take longer. By combining microwave chemistry with bio-mediated techniques, this problem can be solved. The reaction media is quickly and consistently heated by microwave irradiation, creating uniform conditions for nucleation and growth. Microwave heating is a green chemical procedure since it does not emit any potentially hazardous compounds, such as fumes [1,4].

Novel antibacterial and anticancer drugs, such as metallic nanoparticles (M NPs), have piqued the interest of several sectors, including academia and the pharmaceutical business, in this setting. Furthermore, M NPs with positive qualities, namely Ag NPs, have received substantial interest in biomedical and other health-related disciplines in the present world. Ag NPs typically range in size from 1 to 100 nm and exhibit high surface-to-volume ratios [4]. Metabolic compounds from plants such as terpenoids, phenolics, tannins, flavonoids, terpenoids, alkaloids, and polysaccharides have been reported to contribute to the reduction of Ag ions to Ag NPs; thus, the phytochemical composition of each plant differs; however, similarities in structure determine its distinctive features. In essence, physicochemical and technical factors, particularly the size, shape, and stability of Ag NPs, are affected by the technique of extraction, the character of the solvent, the mixing ratio, which is also concentration, pH, and the ambient temperature of the resulting mixtures [5–8]. The size of nanoparticles confers some distinct potential biological features that are valuable in a variety of scientific domains. For the characterization of Ag NPs, numerous approaches are employed to measure particle size, shape, crystal structure, area of the surface, surface volume, and proportion of dimensions. The increasing prevalence of multidrug-resistant bacteria and cancer cases, both of which constitute a serious threat to humanity, necessitates the development of new weapons to attack them. Biogenic Ag NPs are considered to solve this issue [3–10].

The biosynthesis of Ag NPs is considered a green, ecologically friendly, low-cost approach that produces tiny and biocompatible nanostructures with antibacterial, anticancer properties, and potential medical applications. These nanoparticles' biocompatibility is improved by covering them with endogenous biomolecules [1,4–10]. Ag NPs create antiplatelet, antifungal, antiviral, antibacterial, and anti-inflammatory chemicals that are useful against a variety of illnesses [11]. The rising need for non-polluting and hazard-free materials, renewable resources, and eco-friendly solvents has fueled interest in the biogenic synthesis of Ag NPs.

Starch is a natural polymer that is renewable, biodegradable, and abundant, and it has enormous potential for the development of new technologies [12,13]. Furthermore, chemical alterations or the combination of nano-sized additions can improve its mechanical, electrical, optical, and thermal properties, making it more flexible and valuable [14–17]. Potatoes (*Solanum tuberosum* L.) are the subject of the current study as the test material because of their high nutritional content in the form of tubers, global importance as a crop plant, and industrial usability [18]. Starch can be used in the creation of Ag NPs to lessen the potential toxicity of common

reducing agents while also allowing for ecologically friendly synthetic processes [19].

The purpose of this work was to describe the form, size, maximum absorbance, and stabilizing groups of the Ag NPs generated using *S. tuberosum* waste peel. Another aim was to detect AgNPs' antibacterial activity against various bacterial and fungal agents, as well as to assess the cytotoxic activity of the produced Ag NPs against various cancer cell lines. The study's peculiarity is that it identifies a suitable biocompatible herbal reductant for the manufacture of zerovalent silver nanoparticles at a low cost, and the findings are promising. Aqueous $AgNO_3$ and aqueous *Solanum tuberosum* waste peel extract were reduced under ecologically acceptable circumstances to produce colloidal silver nanoparticles (Ag NPs) without the need for a catalyst, template, or surfactant. FTIR, EDX, AFM, TEM, FESEM, and DLS were used to characterize the produced ST-Ag NPs. ST-Ag NPs anticancer efficacy was tested on the HDF, U-118, CaCo2, and Skov-3 cell lines. ST-Ag NPs were examined for their antimicrobial effectiveness towards *E. coli*, *P. aeruginosa*, *B. subtilis*, *S. aureus*, and *C. albicans*, which are responsible for widespread resistant bacterial and fungal infections. Recent studies indicated that synthesized ST-Ag NPs might be highly effective agents in the handling of cancer caused by resistant microorganisms' infectious diseases.

2. Results and discussion

2.1. Spectroscopic data (UV–Vis.)

The color of the reaction mixture changed from brilliant yellow to dark brown, indicating the production of Ag NPs. This color change was caused by the reduction of Ag^+ ions to Ag^0 while transforming to Ag NPs as the creation of vibrations (SPR) on the plasma surface. The conversion of Ag NPs was recorded using UV–Vis spectra at various time intervals (10, 20, 30, 60, and 120 min with 1/1000 dilution). The emergence of a surface Plasmon resonance (SPR) absorption max peak at 453 nm in UV–vis spectroscopy at all-time intervals confirmed the synthesis of ST-Ag NPs (Fig. 1). The band at 453 nm, which is thought to be caused by d-d transitions of the Ag^+ ion, fully vanished following the green synthesis method. This absence demonstrated that the Ag^+ cation was fully diminished [20].

2.2. FE-SEM, TEM, and EDX analysis of biogenic ST-Ag NPs

FE-SEM and TEM images were used to examine the shape and nanoscale dispersion of Ag NPs generated from potato peel waste (Figs. 2 and 3). Examining the micrographs in Fig. 2 showed that the ST-Ag NPs were spherical and stable in appearance. TEM particle measurement, Fig. 3 shows a TEM micrograph of ST-Ag NPs with an average size of 3.91–27.07 nm. In the research conducted by Aktepe and Baran [21] on the *Cucurbita maxima* (CM) plant, the CM-Ag NPs were discovered to be spherical in shape and to have a single distribution. The average particle size of the TEM images of CM-Ag NPs was reported to be 4.41–9.26 nm.

EDX analysis is one of the most effective ways to determine silver nanoparticles' presence in biosynthesis. A large absorption peak at roughly 3 keV was seen, which is typical of the elemental silver created by surface plasmon resonance [22]. The EDX analysis revealed a significant number of strong silver peaks at a ratio of around 85% (Fig. 4). This clearly showed that the *S. tuberosum* leaf extract served as a capping agent on the outside portion of the AgNPs. Weak peaks in the EDX profile were attributed to phytochemicals in the extract, whereas Si was associated with items used to generate the extracts, such as baguettes and petri plates. The EDX profile was evaluated in the investigation on the Black Mulberry plant by Aktepe et al. [23], and a high silver peak was reported, as in the

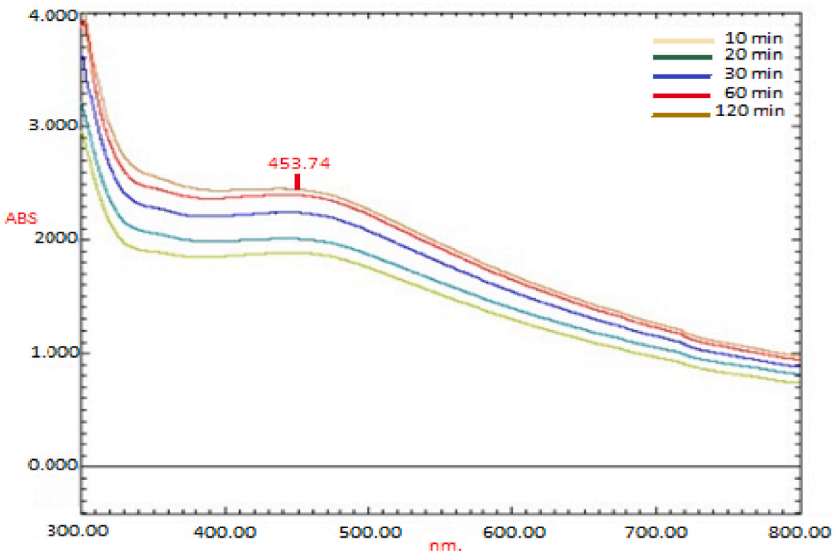

Fig. 1. Time-dependent generation of ST-Ag NPs in UV–Vis spectroscopy and the maximum absorbance value of ST-Ag NPs.

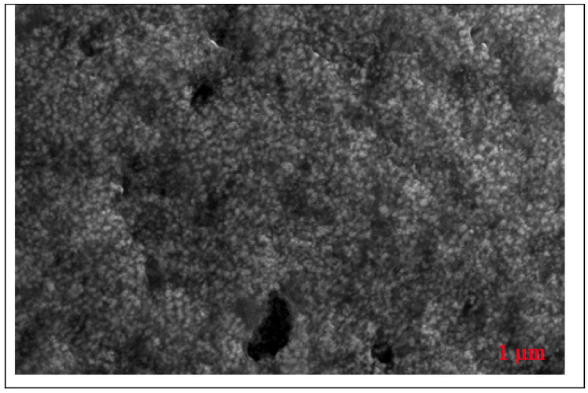

Fig. 2. FE-SEM image of Ag NPs produced from *Solanum tuberosum* aqueous peel extract (at 1 µm).

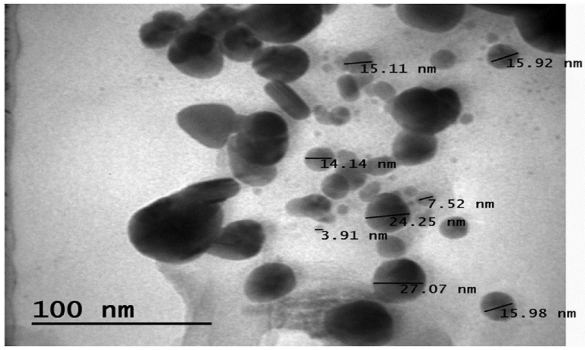

Fig. 3. TEM image of Ag NPs produced from *Solanum tuberosum* plant peel extract.

current work. Also, a silver peak of 3 keV was reported in a separate investigation on *Persea americana* seed extract [24]. Both research findings supported our conclusions.

2.3. Fourier transform infrared spectroscopy (FTIR) result

FT-IR analysis is currently a valuable method for determining the role of functional units in the interaction of metal particles with biological molecules. FT-IR measurements were used to identify potential functional groups in plant phytochemicals that act as reducing, capping, and stabilizing agents in the formation of ST-Ag NP (Fig. 5a and b). *S. tuberosum* aqueous extract and manufactured Ag NPs were compared using FT-IR spectroscopy. Peak value changes suggested that the functional groups were silver-integrated. The frequency measurements were as follows: 3306.06–3307.29 cm^{-1}, 2134.41–2132.03 cm^{-1}, and 1635.09–1635.03 cm^{-1}, respectively. These frequency shifts implied that the bioactive groups implicated in reducing were –OH (hydroxyl) groups, –CN groups, and –C═O carbonyl groups. In a similar work, the functional groups –OH, –CN, and –C═O were shown to be involved in the reduction of NPs formed through *R. acetosella* leaves extract [25]. According to the findings, the likely biomolecules contained in the ST aqueous extract were responsible for the bio-reduction of Ag + ions to Ag NPs and the long-term stability of the generated Ag NPs. Functioning groups such as these may act a critical role in the environmentally friendly production of Ag NPs. However, the probable mechanism is unknown and requires additional exploration.

2.4. Atomic force microscopy (AFM) analysis results

AFM is a method for determining surface height and topography, which indicate surface structure. This approach relates to digital photographs that enable quantitative measurements of surface qualities such as mean square roughness (Rq), mean roughness (Ra), and image analysis from many angles, including 3D simulation. The two-dimensions and three-dimensional shapes of the Ag PNs were characterized using an AFM in non-contact mode. Fig. 6 shows two-dimensional (2D) AFM images of Ag NPs. The well-dispersion of Ag NPs is operated by the balance between the reduction ratio and the phytochemical quantity. The vast majority of phytochemicals will most likely be lost during fractionation, leading to Ag NP aggregation. Fewer reducing species and more capping agents in the leaf extract may result in smaller Ag NPs. The ST-Ag NPs generated were well-balanced and distributed throughout the sample, according to the AFM topography [26,27].

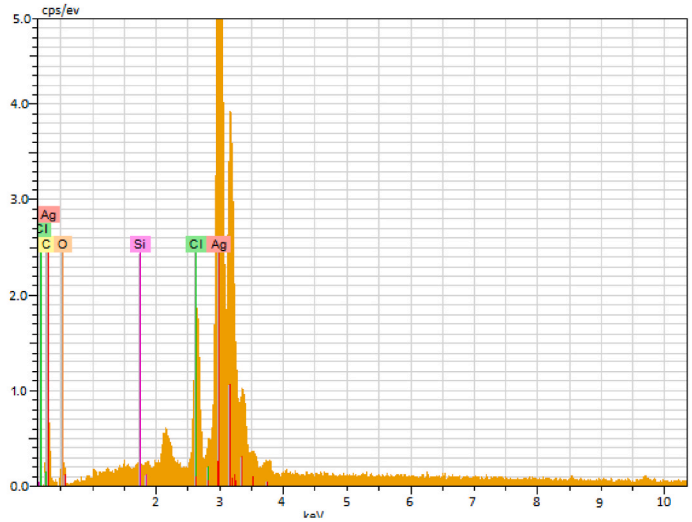

Element	Atomic Number	Series	Weight %	Atomic %
Silver (Ag)	47	L	85.72	44.88
Carbon (C)	6	K	4.82	22.64
Clor (Cl)	17	K	0.47	0.75
Silicium (Si)	14	K	0.02	0.04
Oxygen (O)	8	K	31.68	31.68

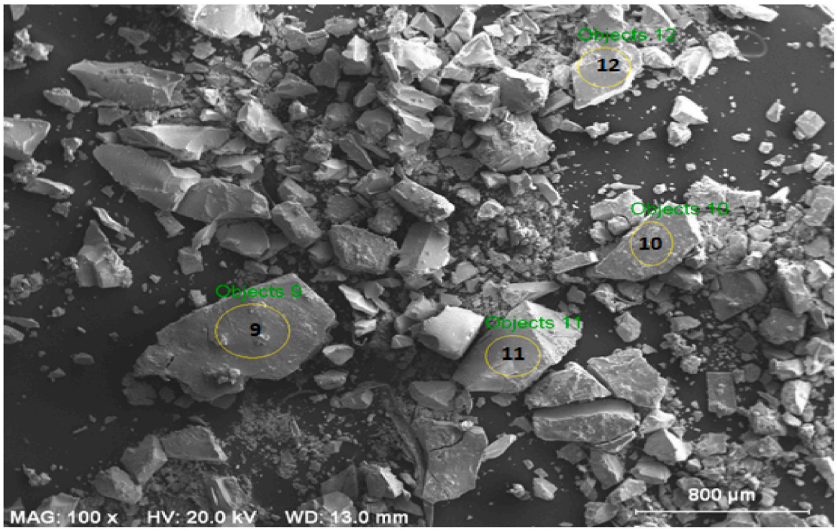

Fig. 4. The EDX spectrum data of Ag NPs synthesized *S. tuberosum* peel aqueous extract.

2.5. X-ray diffraction (XRD) analysis results

The crystal structure and size of the Ag NPs biosynthesis with the peel aqueous extract of *S. tuberosum* were investigated using XRD analysis [28]. The 2θ peak positions were fine specified with the JCPDS NO: 00-004-0783. As shown in Fig. 7, the cubic crystal size of Ag NPs is indicated by the peaks that occur at 111°, 200°, 220°, and 311° equating to 2θ. The crystal size of biologically produced ST-Ag NPs mirrored the values corresponding to these peaks at 2θ as 37.61, 44.72, 64.73, and 77.74, respectively. The XRD analysis indicates that the particles were face-centered cubic (FCC) metallic silver nanoparticles. The average nano size was determined using the highest peak values from the Scherrer equation as 25.22. $D = K\lambda/(\beta \cos \theta)$ [29,30].

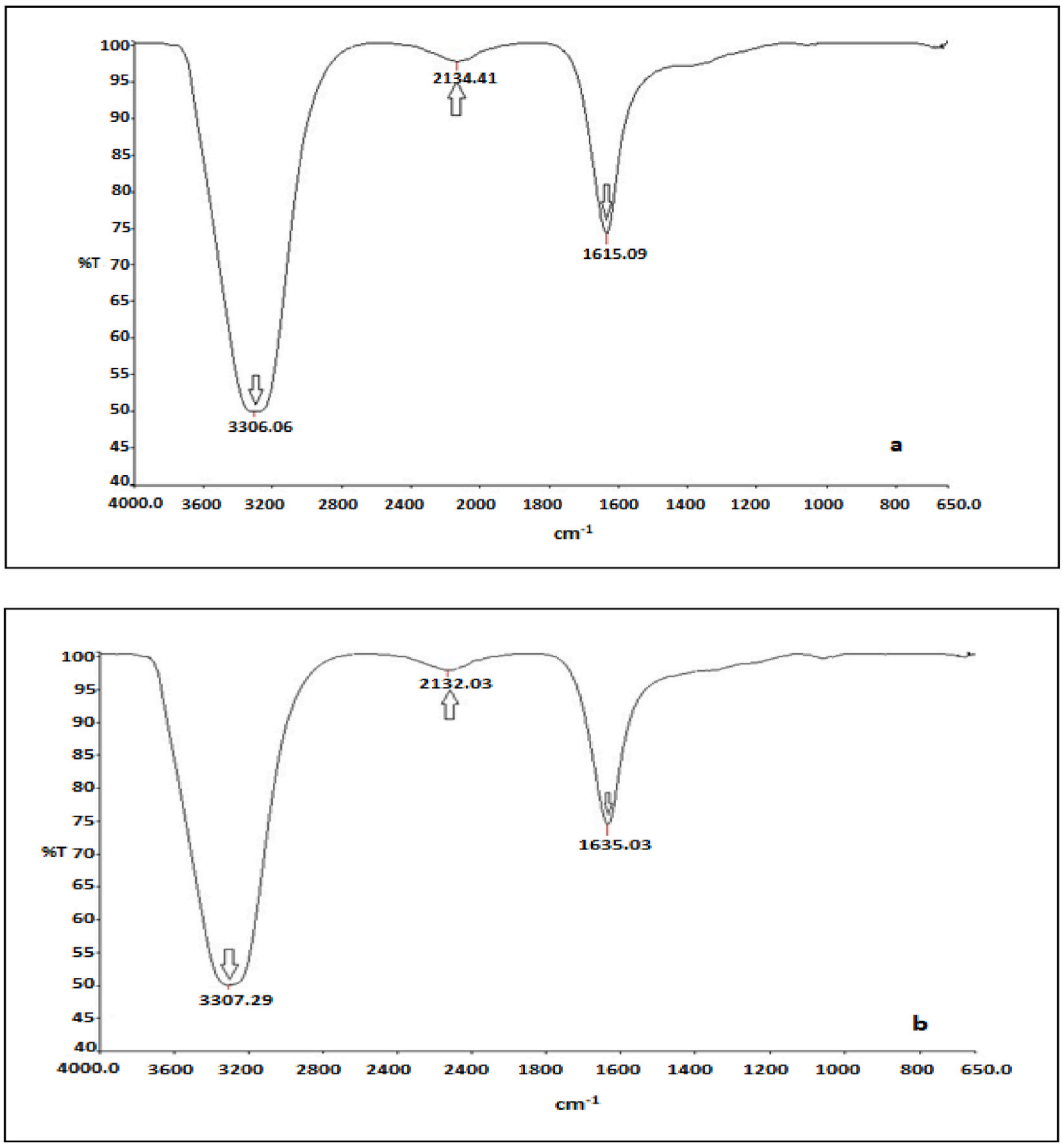

Fig. 5. The FT-IR spectra shown below were used to explore the functional groups implicated in the reductions: a) The FT-IR spectra of *Solanum tuberosum* L. peel aqueous extract, b) FT-IR spectra of the synthesized ST-Ag NPs.

2.6. Zeta potential (ZP), polydispersity index (PDI), and size distribution by intensity results

When evaluating nanoparticle dispersion, effective surface electric charge, and system stability, the zeta potential is an important variable to consider [31]. The ZP is calculated by multiplying the peak area and peak number by the particle charge. The ZP ranges from +100 to −100 mV. A suspension is deemed significantly stable if its ZP is more than +30 mV or less than −30 mV. The ZP is determined not only by the particle's speed in an electric field but also by the viscosity of the dispersion medium [32,33].

ST-Ag NPs were assessed for size (by number distribution), polydispersity index (PDI), and zeta potential. The size of the particle corresponds to the diameter of nanoparticles, and PDI is the measurement that presented us with the size distribution of nanoparticles. The PDI is a dimensionless metric that indicates whether a sample is monodispersing or exhibiting a very wide size distribution. A PDI value less than 0.5 indicates that the particles are monodisperse. Measurements of these parameters are based on a simple principle: for example, by illuminating the sample with a laser and adjusting the detector position to 173° or 90° depending on the Zetasizer Nano model, analysis can be performed.

In this study, the detection angle was set to 173° to analyze scattered light. Another feature that can be detected using DLS is the zeta potential (ζ), which simply consists of sensing electrostatic/charge at the surface of the nanoparticle using a laser that passes through the sample cell. The zeta potentials of the ST-AgNPs were measured at 25 °C. The zeta potential is an examination of the surface charge of Ag NPs that is used to change their stability via electrostatic repulsion. Data were taken using dynamic light

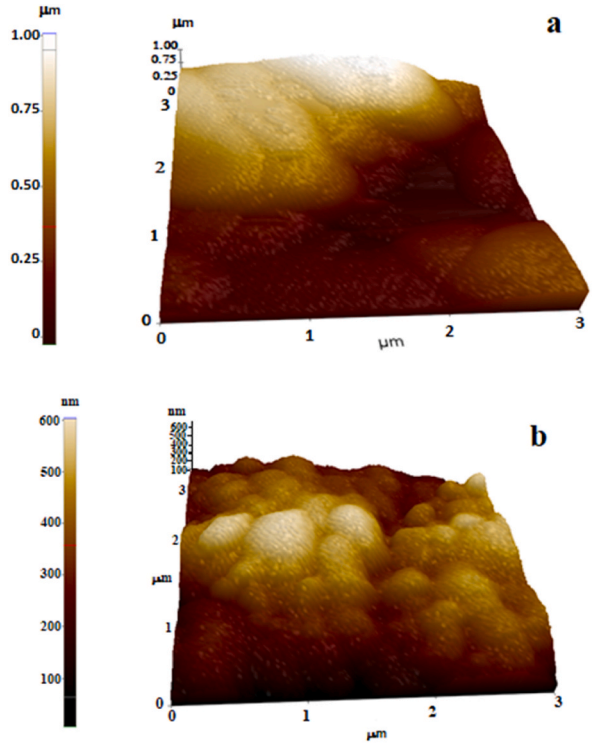

Fig. 6. AFM topography of ST-Ag NPs synthesized by *Solanum tuberosum* peel aqueous extract (a) and corresponding 3D topography image (b).

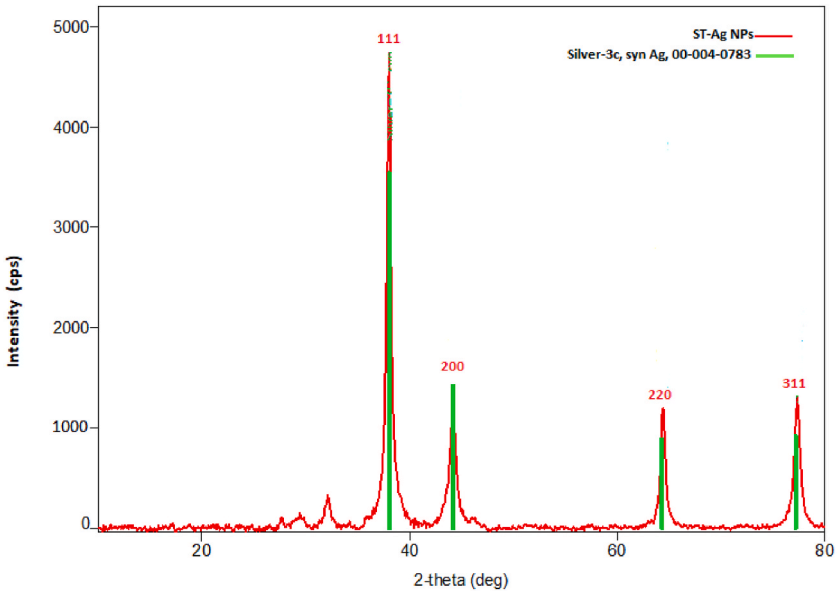

Fig. 7. The crystal shape of biocompatible synthesis ST-Ag NPs is depicted by X-ray diffraction.

scattering (DLS) 3–4 h after the nanoparticles were synthesized. The mean hydrodynamic size of the polydisperse Ag NPs suspension was found to be 323.5 nm; this is substantially greater than the TEM results. The mean size in DLS was calculated utilizing dynamic light dispersed from the core particles and a coating of bioactive plant extract components around the silver nanocore. The −31.3 mV zeta potential value indicates the stability of the produced ST-Ag NPs. In photon correlation spectroscopy, the polydispersity index (PDI Index) is a metric used to characterize particle size distributions. It is given as a dimensionless number extrapolated from the autocorrelation function. The polydispersity index (PDI) score can range from 0.01 (monodispersed particles) to 0.5–0.7, with 0.7

indicating that the formulation has a wide particle size dispersion. The PDI value of ST-Ag NPs was also determined to be 0.459. The negative value represents the negative charge that has been generated on the surface of nanoparticles. Fig. 8 depicts the specifics of the DLS and zeta potential measurements of Ag NPs [29].

2.7. TGA-DTA analysis results of the ST-Ag NPs

The TGA curve depicts the percentage of mass loss that the synthesized ST-Ag NPs experience as temperatures rise, whereas the DTA curve depicts the temperature at which the quickest degradation happens at each step of degradation as temperatures rise (Fig. 9) [34].

When the TGA-DTA curve was analyzed, it was possible to deduce that the mass loss of 0.441 mg at 46–218 °C was due to moisture, the mass loss of 1.36 mg at 218–513 °C was due to hydrated water, and the mass loss of 0.463 mg at 513–896 °C was a result of the mass loss of phytochemicals. Even at 900 °C, it was found that only 25% of the produced Ag NPs had been degrading. This suggests that the nanoparticles created are important in terms of stability and endurance and that they can be usefully utilized in the coating business in the future. It is observed that the present study is consistent with other similar studies and the findings overlap with previous studies [35,36].

2.8. Evaluation of the antimicrobial activities of ST-Ag NPs

Both the gram-positive and negative bacterial strains and the yeast were cultured in the MHB for 24 h at 37 °C until turbidity (0.5 McFarland) reached approximately 10^8 CFUs mL-1. The microdilution test was used to measure the MIC of the produced ST-Ag NPs. The bio-synthesized ST-Ag NPs were then serially diluted twice in a sterile MHB medium. Following that, 100 μl of the ST-Ag NPs dilutions was put into a 96-well microplate, inoculated with 100 μl of the selected microbial strains to a final concentration of, and incubated at 37 °C (with shaking) a day. The minimum inhibitory concentration (MIC) of bio-synthesized ST-Ag NPs was determined as the lowest concentration at which pathogenic bacteria growth was inhibited after the incubation period (24 h, 37 °C).

A comparison was made between the antimicrobial effects of silver nanoparticles and the MIC (lowest concentration at which microorganism growth is inhibited) values of 1 mM silver nitrate and commercial antibiotics. The effects of ST-Ag NPs on Gram (+) (*S. aureus* ATCC 29213: 0.225 μg $mL^{-1}$and *B. subtilis* ATCC 11773: 0.425 μg/mL) and Gram (−) (*E. coli* ATCC 25922: 1.75 μg/mL,

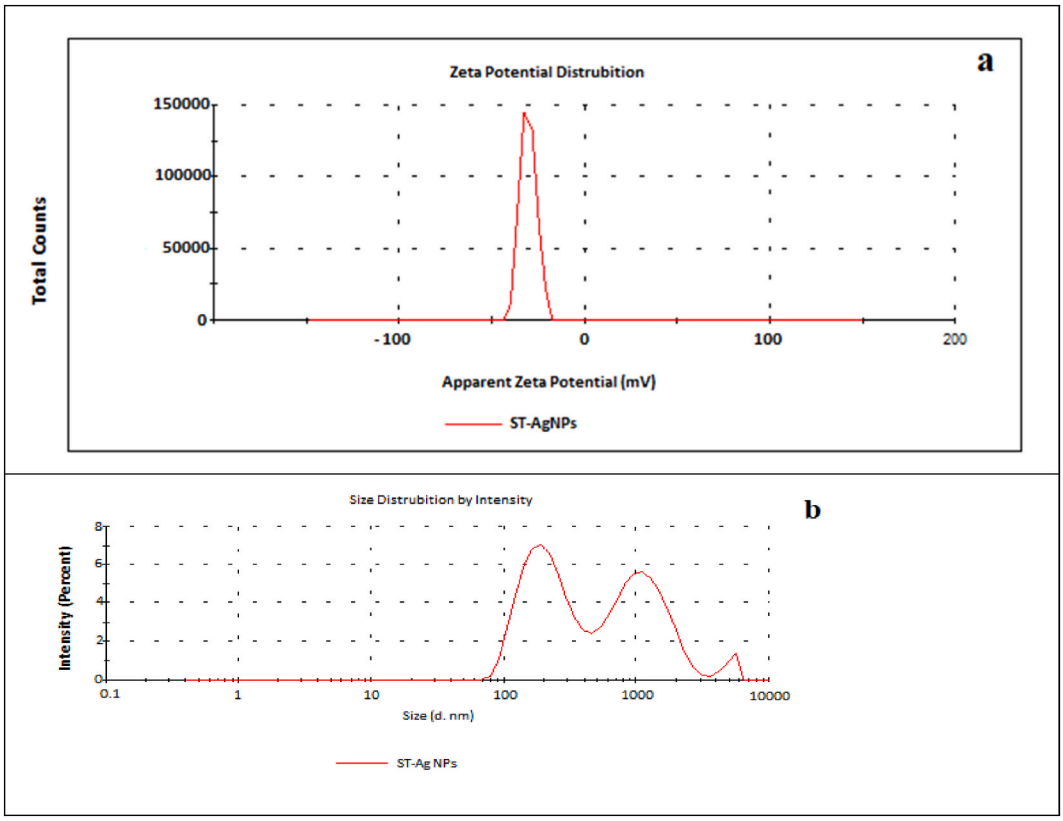

Fig. 8. (**a**) Surface charge distribution of synthesized ST-Ag NPs obtained through zeta potential analysis data and (**b**) Average size distributions of synthesized ST-Ag NPs by DLS depending on the density.

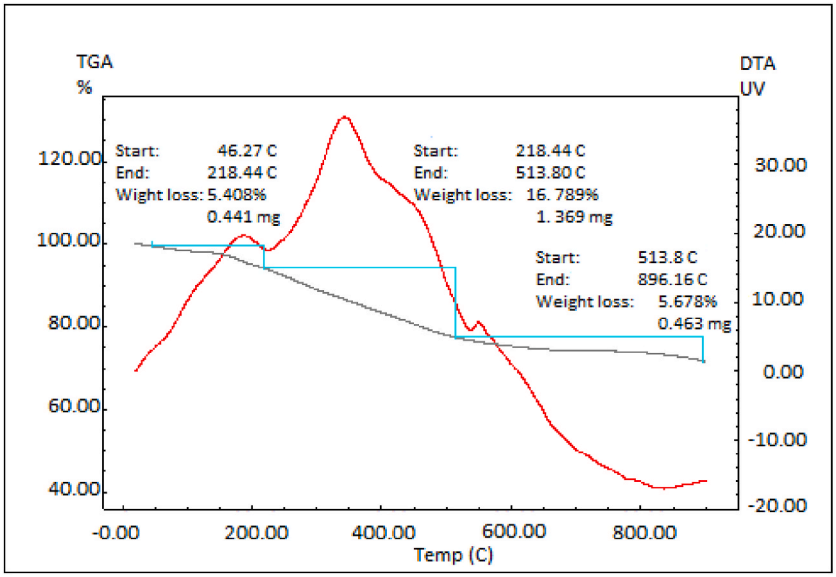

Fig. 9. TGA-DTA results of the biosynthesized ST-Ag NPs.

P. aeruginosa ATCC27833: 0.85 μg/mL) bacterial strains and *C. albicans* yeast were examined (Table 1).

When the effects of standard antibiotics, silver nitrate solution, and ST-Ag NPs were compared, it was revealed that the ST-Ag NPs had more effective inhibitory activities on the pathogen microorganisms at lower concentrations (Table 1). Silver nanoparticles (Ag NPs) have been shown to be one of the most efficient antibacterial and anticancer agents among the many types of biosynthesized metallic and metal oxide NPs due to their exceptional characteristics [36,37]. A possible mechanism for effective attachment between the positive surface charge of Ag NPs and the negative surface charge of bacteria was described. This connection breaks down the bacterium's cell wall, causes protein degradation and fracture, and ultimately results in necrosis and death [38]. Both a low and high density of plant compounds surrounding the NPs can have an effect on the degree to which the bacteria can access the antibiotic. In this case, the low density of plant metabolites around the NPs might offer a favorable domain for antibiotic binding to the nanoparticles [39,40].

2.9. Cytotoxic activity of ST-AgNPs

Due to their distinct physicochemical features, silver and gold nano biomaterials are thought to be extremely valuable materials for the treatment of specific types of cancer in addition to already available nano platforms like liposomes and dendrimers intended for cancer treatments. These nano-biomaterials can be created as smart nano-drugs for therapeutic and diagnostic uses since they were created using biosynthetic methods. Nano biomaterials made of silver and gold have a lot of potential as targeted medication delivery systems [41]. Nanomaterials can be coupled with diagnostic and/or therapeutic chemicals for theranostic applications. Metallic nanoparticles (NPs), which are among the many various types of nanomaterials, have sparked a lot of interest in a number of applications due to their distinctive optical, electrical, physical, chemical, and biological characteristics [42]. Several recent studies indicate that metal nanoparticles can inhibit the growth of certain cancer cell types. The mechanism of Ag NPs toxicity is related to the disintegration of lipoteichoic acid, peptidoglycan, and phosphatidyle thanol amine, which causes reactive oxygen radicals to cause damage. As the production of fatal quantities of ROS such as superoxide (O_2) and hydroxyl (•OH). Ag NPs produce Ag^+ in mitochondria and nucleus, causing cell damage and apoptosis. Ag NPs were reported to have minimal toxicity in healthy human cells [43–45]. The cytotoxic effects of the Ag NPs produced from *S. tuberosum* peel extracts were evaluated on the Skov-3, Caco-2, U118, and HDF cell lines at various concentrations, which can be seen in Fig. 10.

During the course of the experiment, a variety of concentrations ranging from 0 (Control) to 100 μg/mL were used. According to the results of the MTT analysis data, ST-Ag NPs decreased the viability of the U118, Caco-2 Skov-3, and HDF cell lines in a dose-dependent

Table 1
Antimicrobial effects of AgNPs, Silver Nitrate solution, and antibiotics on microorganisms.

Organism	ST-Ag NPs	Silver Nitrate	Antibiotic (μg/ml)
S. aureus	0.225	2.65	2
B. subtilis	0.425	1.32	1
P. aeruginosa	0.850	1.32	4
E. coli	1.750	0.66	2
C. albicans	3.50	0.66	2

manner, with the 50% inhibition concentration (IC_{50}) displayed in Table 2. However, in relation to the proliferative effect of NPs on U118 cells at 200 μg/mL, an increase was observed in the % viability of the cells. The cellular absorption of NPs and their anticancer activity have been shown to differ depending on the nanoparticle's size, charge, shape, and surface area, as well as the cell type being treated. Cancer cells have distinct growth properties than normal cells, which accounts for the variation in cytotoxic action.

Cancer-related leaky blood arteries (pore diameters of 100–600 nm) enable NPs to infiltrate into cancer cells. The content, size, and dosage of NPs all have a role in producing toxicity in cancer cells. The different rates of metabolism and cell proliferation may be to blame for the proliferative activity of the Ag NPs [44–46]. At doses ranging from 1 μg/mL to 100 μg/mL, ST-Ag NPs had a mild cytotoxic impact on HDF cells (Fig. 10). These findings suggest that ST-Ag NPs may not be hazardous to normal cell conditions.

3. Materials and methods

3.1. Materials and extraction process

For the reduction process, $AgNO_3$ salt was commercially obtained from Merck, Germany. *Solanum tuberosum* (ST) was obtained from the local market of the Adilcevaz district of Bitlis. The ST peels were dried (room condition; 25 ± 2 °C) after being washed repeatedly with pure water to get rid of any clinging contaminants. Then, 750 mL of deionized water and 200 g of powdered peel material were combined and brought to a boil at 75 °C. The extract was cooled after boiling and then put onto a 0.45 mm membrane filter. For the following process, the cooled filtrate was kept in a freezer at 4 °C.

3.2. Silver nanoparticle synthesis

First, a solid $AgNO_3$ salt was dissolved in water to make an aqueous solution of 40 mM $AgNO_3$. The 50 mL of 40 M $AgNO_3$ solution and 750 mL ST extracts were left to react in a medium at a ratio of 15:1 at room temperature. Wavelength scanning (UV–vis spectroscopy) was done at different time intervals (10, 20, 30, 60, and 120 min) depending on the degree of color change for determining the maximum absorbance of biologically generated ST-Ag NPs. The solution, which had darkened with time, was centrifuged (4500 rpm, 15 min) at the final stage of the synthesis. The nanoparticles fell to the bottom, and the supernatant was discarded. The plant extract was subsequently removed from the produced nanoparticles by washing them 10 times with distilled water. The resulting solid portion (ST-Ag NPs) was subsequently dried in an oven (60 °C, 24 h).

3.3. Instrumentation

Four mg of ST-Ag NPs were dissolved in 20 mL of distilled water and sonicated for 20 min. After that, the combination was examined using UV–Vis spectrophotometry. The mixture's pH was adjusted to 7.0 by adding 1 N sodium hydroxide solution. The maximum absorbance of the produced ST-Ag NPs was measured using a spectrophotometer (Agilent CARY 60) between 300 and 800 nm [20,23]. Transmission electron microscopy (HITACHI 7700), electron dispersive X-ray (Quanta FEG240), field emission scanning electron microscopy (FE-SEM) (Quanta FEG240), atomic force microscopy (AFM), and X-ray diffraction analysis (Rad B-DMAX II) were used to determine the size, surface distribution, morphology, and crystal structure of Ag NPs. The XRD equipment was used to examine

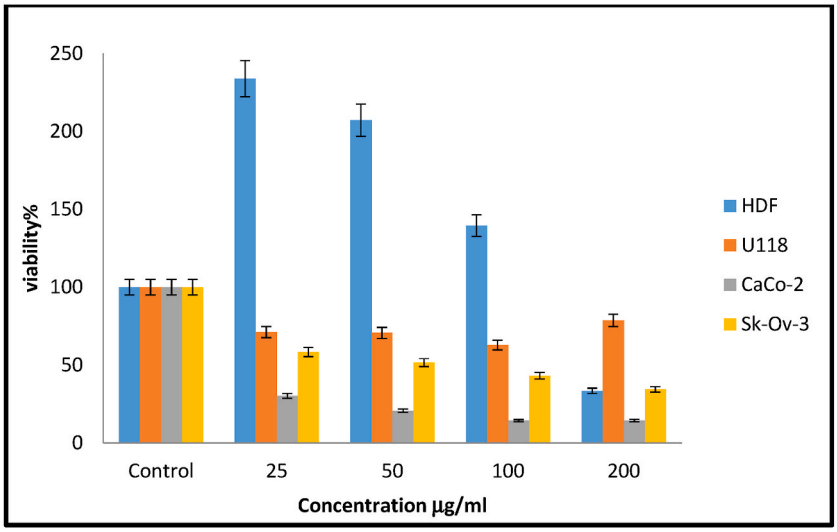

Fig. 10. Cell line viability levels following 48 h of association with HDF, U118, Caco-2, and Skov-3 cell lines as a consequence of ST-Ag NPs cytotoxicity. (For 48 h, cells (1×10^5 cells/well) were treated with the specified doses of ST-Ag NPs. A colorimetric test utilizing MTT solution was used to measure cell viability%. The standard deviation (n = 3) was represented by the error bars.).

Table 2
Cell line % viability rates following 48 h of contact with biosynthesis ST-Ag NPs (n = 3).

	Control	25 μg/mL	50 μg/mL	100 μg/mL	200 μg/mL	IC_{50}
HDF	100	233.79 ± 0.72	207.10 ± 0.64	139.48 ± 0.43	33.48 ± 0.10	43.39 ± .0.28
Caco-2	100	30.24 ± 0.38	20.67 ± 0.26	14.35 ± 0.18	14.39 ± 0.18	6.43 ± 0.18
U118	100	71.09 ± 1.29	70.63 ± 0.91	62.80 ± 0.91	78.64 ± 0.81	23.37 ± 0.23
Skov-3	100	58.33 ± 0.80	51.54 ± 0.70	43.14 ± 0.59	34.36 ± 0.47	4.31 ± 0.15

the crystal patterns and crystal sizes of the nanoparticles generated during the synthesis. Using the Debye-Scherrer formula ($D = K\lambda/(\beta \cos \theta$; D = the size of the particle, K = constant value, λ = X-ray wavelength, β = half peak width (radians) of maximum intensity peak, θ = XRD diffraction angle of the maximum intensity peak) and XRD findings in the range of 20–80 at 2 theta, the crystal nanosized of the ST-Ag NPs generated after synthesis was determined [34,36]. Nanosizer was also used to determine nanoparticle zeta potential, particle size, and polydispersity index (PDI). The absorption spectra acquired with the FTIR device can provide information about the structure of a produced molecule. The different functional groups in the produced ST-Ag nanoparticles were identified by FTIR analysis [30]. A 50 mL Ag NP colloidal solution was prepared for the FTIR experiment utilizing optimum conditions (1 mM $AgNO_3$; 5% EFE) and centrifuged at 10.000 rpm for 25 min. After that, the pellet was resolved in 5 mL of pure water and dried for 24 h. FT-IR spectroscope (Agilent Carry 360) spectra from 4000/cm to 450/cm were acquired with a resolution of 2 cm and 5 scans/sample using 1 mg of finely milled Ag NPs generated with 200 mg of KBr. For thermogravimetric (TGA) and differential thermal analysis (DTA) experiments, 5 mg of lyophilized Ag NPs were utilized [47–49].

3.4. Antimicrobial activities of ST-Ag NPs

Pathogen gram-negative (*P. aeruginosa* and *E. coli*) and gram-positive (*B. subtilis* and *S. aureus*) bacterial strains, as well as yeast (*C. albicans*), were employed to study the antipathogenic properties of the bio-derived ST-Ag NPs. The minimum inhibitory concentration (MIC) approach was used to assess antipathogenic activity. Pathogenic microbial strains were cultured in Muller-Hinton broth (MHB) medium for 24 h at 37 °C to determine antimicrobial activity, and turbidity was adjusted to about 10^8 CFU mL-1 after the incubation time. Furthermore, successive dilutions of the created Ag NPs were prepared for future tests by dissolving them in clean water. Fluconazole was utilized to treat yeast (*Candida albicans*), whereas colistin and vancomycin medicines were used to treat gram (−) and gram (+) bacteria, respectively. By measuring how rapidly the germs proliferated in the agar broth, the CLSI M07-A8 standard broth dilution technique was utilized to examine the antibacterial and antifungal effects of Ag NPs.

3.5. Cytotoxicity analysis of ST-AgNPs

Glioblastoma cells (U118), human colorectal adenocarcinoma (Caco-2), dermal fibroblasts (HDF), and human ovarian adenocarcinoma cells (Skov-3), cell lines were plated individually using 96-well plates with the concentration of (1×10^4 cells/well) in DMEM media with antibiotic-antimycotic solution (1×) and 10% FBS (Merck KGaA, Darmstadt, Germany) in a CO_2 incubator (5% CO_2) at 37 °C. After washing up the cells with 200 μL of 1× FBS, they were treated with various concentrations of ST-Ag NPs (25, 50, 100, and 200 μg/mL). The plate system was replaced in an incubator for 48 h. After incubation, MTT [3-(4.5-dimethyldithiazol-2-yl)-2.5 diphenyl tetrazolium bromide] solution was added to each and every well. On a CO_2 incubator, the plate was kept in the dark for 3 h inside the incubator at 37 °C. The supernatant was removed after 3 h, and the purple-blue color production was diluted with 100 mL of DMSO. At 540 nm, the absorbance was measured with MultiScan Go (Thermo) equipment. The percentages of cell viability were estimated using the formula% viability = U/C*100 [50,51]. The absorbance values of cells treated with Ag NPs are represented by U, whereas the absorbance values of control cells are represented by C.

4. Conclusions

Cancer is the top cause of mortality recorded. Cancer-related fatalities were documented in the lung, liver, stomach, colon, and breast. Overall, Asia, Africa, and America account for 70% of all cancer fatalities and 60% of all cancer cases recorded worldwide. Cancer therapies are currently delivered by surgery, radiation, and chemotherapy. Also, with the increased use of antibiotics for the treatment of a variety of pathogenic conditions, multidrug resistance is on the rise. The use of antibiotics with a wide spectrum has resulted in resistance to several of the microbiological human diseases that pose a significant threat to humanity. In certain areas, more than 25% resistance was observed in invasive staphylococcal isolates known as methicillin-resistant *Staphylococcus aureus*, indicating that these organisms required an effective medication to manage. *C. albicans* strains are resistant to fluconazole, a routinely used antimycotic medicine. The rise of resistant viral strains is causing major issues in antiretroviral therapy, especially in the case of HIV. Similar resistance issues have been identified in plant-infecting diseases. As a result, there is an urgent need for innovative treatment and control options for these pathogenic infections. The improvement of environmentally friendly methods for the production of nanoparticles is gaining traction. The lack of harmful chemicals in the synthesis process, as well as the lower cost and ease of manufacturing, provides a significant benefit for biological synthesis. The current work employed an aqueous extract of Solanum tuberosum waste peel in conjunction with a simple, green, and effective approach that was used to create silver nanoparticles at room temperature and without the use of potentially dangerous lowering agents throughout the biosynthesis process. Green synthesis silver

nanoparticles were revealed to be composed of round and oval particles with a crystalline structure. Furthermore, the biogenic ST-Ag NPs were exhibited cytotoxic to the U118, Caco-2, and Skov-3 cancerous cell lines, as well as had high antibacterial properties against bacterial strains and yeast. Finally, green-generated silver and silver oxide nanoparticles derived from the peel of *Solanum tuberosum* are attractive candidates for antibacterial and anticancer applications in the biomedical and agricultural industries.

Funding

Scientific Research and Innovation Foundation of the First Affiliated Hospital of Harbin Medical University (2021M05, DH).

Institutional review board statement

Not applicable.

Informed consent statement

Not applicable.

Sample availability

Samples of the compounds of ST-Ag NPs are available from the corresponding authors.

Author contribution statement

Jiajun Xu: Ayşe Baran: Mehmet Fırat Baran: Deniz Bariş Cebe: Beşir Dağ: Performed the experiments; Wrote the paper.
Mahmut Yıldıztekin: Performed the experiments; Analyzed and interpreted the data; Wrote the paper.
Canan Aytuğ Ava: Sevgi İrtegün Kandemir: Analyzed and interpreted the data; Wrote the paper.
Dayong Han: Cumali Keskin: Aziz Eftekhari: Conceived and designed the experiments; Contributed reagents, materials, analysis tools or data; Wrote the paper.
Aferin Beilerli: Rovshan Khalilov: Contributed reagents, materials, analysis tools or data; Wrote the paper.

Data availability statement

Data will be made available on request.

Additional information

No additional information is available for this paper.

Declaration of competing interest

The authors declare that they have no known competing financial interests or personal relationships that could have appeared to influence the work reported in this paper.

Acknowledgments

Not applicable.

References

[1] A. Nasibova, Generation of nanoparticles in biological systems and their application prospects, Advances in Biology & Earth Sciences 2 (2023) 140–146.
[2] D.M. Cruz, E. Mostafavi, A. Vernet-Crua, H. Barabadi, V. Shah, J.L. Cholula-Díaz, T.J. Webster, Green nanotechnology-based zinc oxide (ZnO) nanomaterials for biomedical applications: a review, JPhys Materials 3 (2020), 034005, https://doi.org/10.1088/2515-7639/ab8186.
[3] G.Y. Gunashova, Synthesis of silver nanoparticles using a thermophilic bacterium strain isolated from the spring Yukhari istisu of the Kalbajar region (Azerbaijan), Advances in Biology and Earth Sciences 3 (2022) 198–204.
[4] A.M. El-Khawaga, A. Zidan, A.I. Abd El-Mageed, Preparation methods of different nanomaterials for various potential applications: a Review, J. Mol. Struct. 1281 (2023), 135148, https://doi.org/10.1016/j.molstruc.2023.135148.
[5] A. Balciunaitiene, P. Viskelis, J. Viskelis, P. Streimikyte, M. Liaudanskas, E. Bartkiene, V. Lele, Green synthesis of silver nanoparticles using extract of *Artemisia absinthium* L., *Humulus lupulus* L. and *Thymus vulgaris* L., physico-chemical characterization, antimicrobial and antioxidant activity, Processes 9 (2021) 1304, https://doi.org/10.3390/pr9081304.
[6] G.Y. Gunashova, F.R. Ahmadova, R.I. Khalilov, Biosynthesis of silver nanoparticles using thermophilic Bacillus Sp. Б1, Advances in Biology & Earth Sciences 2 (2021) 142–145.
[7] V.N. Ramazanli, Effect of ph and temperature on the synthesis of silver nano particles extracted from olive leaf, Advances in Biology & Earth Sciences 2 (2021).
[8] N.K. Sharma, J. Vishwakarma, S. Rai, T.S. Alomar, N. AlMasoud, A. Bhattarai, Green route synthesis and characterization techniques of silver nanoparticles and their biological adeptness, ACS Omega 7 (31) (2022) 27004–27020, https://doi.org/10.1021/acsomega.2c01400.

[9] H. Barabadi, A. Mohammadzadeh, H. Vahidi, M. Rashedi, M. Saravanan, N. Talank, A. Alizadeh, Penicillium chrysogenum-derived silver nanoparticles: exploration of their antibacterial and biofilm inhibitory activity against the standard and pathogenic Acinetobacter baumannii compared to tetracyclineJ, Clust. Sci 33 (2022) 1929–1942, https://doi.org/10.1007/s10876-021-02121-5.

[10] A.F. Jafarova, V.N. Ramazanli, Antibacterial characteristics of ag nanoparticle extracted from olive leaf, Advances in Biology & Earth Sciences 3 (2020).

[11] R. Arif, R. Uddin, A review on recent developments in the biosynthesis of silver nanoparticles and its biomedical applications, Med. Devices Sens. 4 (2021), e10158, https://doi.org/10.1002/mds3.10158.

[12] S. Ahmad, S. Munir, N. Zeb, A. Ullah, B. Khan, J. Ali, M. Bilal, M. Omer, M. Alamzeb, S.M. Salman, S. Ali, Green nanotechnology: a review on green synthesis of silver nanoparticles-An ecofriendly approach, Int. J. Nanomed. 14 (2019) 5087, https://doi.org/10.2147/IJN.S200254.

[13] L. Castillo-Henríquez, K. Alfaro-Aguilar, Ugalde-Álvarez, J. Vega-Fernández, L. Montes de Oca-Vásquez, G. Vega-Baudrit, J.R, Green synthesis of gold and silver nanoparticles from plant extracts and their possible applications as antimicrobial agents in the agricultural area, Nanomater 10 (2020) 1763, https://doi.org/10.3390/nano10091763.

[14] A. Naganthran, G. Verasoundarapandian, F.E. Khalid, M.J. Masarudin, A. Zulkharnain, N.M. Nawawi, S.A. Ahmad, Synthesis, characterization and biomedical application of silver nanoparticles, Materials 15 (2022) 427, https://doi.org/10.3390/ma15020427.

[15] M. Ijaz, M. Zafar, T. Iqbal, Green synthesis of silver nanoparticles by using various extracts: a review, Inorg. Nano-Met. Chem. 51 (2020) 744–755, https://doi.org/10.1080/24701556.2020.1808680.

[16] T.V.M. Sreekanth, P.C. Nagajyothi, N. Supraja, T.N. Prasad, V. K.V, Evaluation of the antimicrobial activity and cytotoxicity of phytogenic gold nanoparticles, Appl. Nanosci. 5 (2015) 595–602, https://doi.org/10.1007/s13204-014-0354-x.

[17] M.R. Bindhu, M. Umadevi, G.A. Esmail, N.A. Al-Dhabi, M.V. Arasu, Green synthesis and characterization of silver nanoparticles from Moringa oleifera flower and assessment of antimicrobial and sensing properties, J. Photochem. Photobiol. B Biol. 205 (2020), 111836, https://doi.org/10.1016/j.jphotobiol.2020.111836.

[18] P.Ł. Kowalczewski, A. Olejnik, S. Świtek, A. Bzducha-Wróbel, P. Kubiak, M. Kujawska, G. Lewandowicz, Bioactive compounds of potato (Solanum tuberosum L.) juice: from industry waste to food and medical applications, Crit. Rev. Plant Sci. 41 (2022) 52–89, https://doi.org/10.1080/07352689.2022.2057749.

[19] J. Waterschoot, S.V. Gomand, F. Fierens, J.A. Delcour, Production, structure, physicochemical and functional properties of maize, cassava, wheat, potato and rice starches, Starch Staerke 67 (2015) 14–29, https://doi.org/10.1002/star.201300238.

[20] N. Aktepe, N. Erbay, A. Baran, M.F. Baran, C. Keskin, Synthesis, characterization, and evaluation of the antimicrobial activities of silver nanoparticles from *Cyclotrichium origanifolium* L, Int. J. Agric. Environ. Food Sci. 6 (2022) 426–434, https://doi.org/10.31015/jaefs.2022.3.12.

[21] N. Aktepe, A. Baran, Green synthesis and antimicrobial effects of silver nanoparticles by pumpkin *Cucurbita maxima* fruit fiber, Med. Sci. 11 (2022) 794–799, https://doi.org/10.5455/medscience.2022.02.036.

[22] M. Naveed, H. Batool, S.U. Rehman, A. Javed, S.I. Makhdoom, T. Aziz, M. Alhomrani, Characterization and evaluation of the antioxidant, antidiabetic, anti-inflammatory, and cytotoxic activities of silver nanoparticles synthesized using *Brachychiton populneus* leaf extract, Processes 10 (2022) 1521, https://doi.org/10.3390/pr10081521.

[23] N. Aktepe, A. Baran, M.N. Atalar, M.F. Baran, C. Keskin, M.Z. Düz, Ö. Yavuz, S.I. Kandemir, D.E. Kavak, Biosynthesis of black mulberry leaf extract and silver nanoparticles (Ag NPs): characterization, antimicrobial and cytotoxic activity applications, MAS J. Appl .Sci. 6 (2021) 685–700, https://doi.org/10.52520/masjaps.120.

[24] G. Rajkumar, R. Sundar, Biogenic one-step synthesis of silver nanoparticles (AgNPs) using an aqueous extract of Persea americana seed: characterization, phytochemical screening, antibacterial, antifungal and antioxidant activities, Inorg. Chem. Commun. 143 (2022), 109817, https://doi.org/10.1016/j.inoche.2022.109817.

[25] N. Aktepe, H. Bütüner, A. Baran, M.F. Baran, C. Keskin, Synthesis, Characterization and evaluation of antimicrobial activities of silver nanoparticles obtained from *Rumex acetosella* L. (Sorrel) plant, Int. J. Agric. Environ. Food Sci. 6 (2022) 522–529, https://doi.org/10.31015/jaefs.2022.4.4.

[26] R.S. Priya, D. Geetha, P.S. Ramesh, Antioxidant activity of chemically synthesized AgNPs and biosynthesized *Pongamia pinnata* leaf extract mediated AgNPs - a comparative study, Ecotoxicol. Environ. Saf. 134 (2016) 308–318, https://doi.org/10.1016/j.ecoenv.2015.07.037.

[27] V. Kumar, S.C. Yadav, S.K. Yadav, *Syzygium cumini* leaf and seed extract mediated biosynthesis of silver nanoparticles and their characterization, J. Chem. Technol. Biotechnol. 85 (2010) 1301–1309, https://doi.org/10.1002/jctb.2427.

[28] X. Huang, R. Wang, T. Jiao, G. Zou, F. Zhan, J. Yin, L. Zhang, J. Zhou, Q. Peng, Facile preparation of hierarchical AgNP-loaded MXene/Fe_3O_4/polymer nanocomposites by electrospinning with enhanced catalytic performance for wastewater treatment, ACS Omega 4 (2019) 1897–1906, https://doi.org/10.1021/acsomega.8b03615.

[29] C. Keskin, M.N. Atalar, M.F. Baran, A. Baran, Environmentally friendly rapid synthesis of gold nanoparticles from *Artemisia absinthium* plant extract and application of antimicrobial activities, JIST 11 (2021) 365–375, https://doi.org/10.21597/jist.779169.

[30] A. Baran, M.F. Baran, C. Keskin, S.I. Kandemir, M. Valiyeva, S. Mehraliyeva, R. Khalilov, Eftekhari, A. Ecofriendly/rapid synthesis of silver nanoparticles using extract of waste parts of artichoke (*Cynara scolymus* L.) and evaluation of their cytotoxic and antibacterial activities, J. Nanomater. 2021 (2021), 2270472, https://doi.org/10.1155/2021/2270472.

[31] Y. Zhang, N. Kohler, M. Zhang, Surface modification of superparamagnetic magnetite nanoparticles and their intracellular uptake, Biomaterials 23 (2022) 1553–1561, https://doi.org/10.1016/S0142-9612(01)00267-8.

[32] D.K. Naser, A.K. Abbas, K.A. Aadim, Zeta potential of Ag, Cu, ZnO, CdO and Sn nanoparticles prepared by pulse laser ablation in liquid environment, Iraqi J. Sci. 61 (2020) 2570–2581, https://doi.org/10.24996/ijs.2020.61.10.13.

[33] S. Jana Singla, A. Thakur, R. Kumari, C. Goyal, S. Pradhan, J. Green synthesis of silver nanoparticles using *Oxalis griffithii* extract and assessing their antimicrobial activity, OpenNano 7 (2022), 100047, https://doi.org/10.1016/j.onano.2022.100047.

[34] M.F. Baran, C. Keskin, A. Baran, A. Hatipoğlu, M. Yildiztekin, S. Küçükaydin, A. Eftekhari, Green synthesis of silver nanoparticles from *Allium cepa* L. Peel extract, their antioxidant, antipathogenic, and anticholinesterase activity, Molecules 28 (2023) 2310, https://doi.org/10.3390/molecules28052310.

[35] A.K. Singh, R. Tiwari, V. Kumar, P. Singh, S.K. Riyazat Khadim, A. Tiwari, V. Srivastava, S.H. Hasan, R.K. Asthana, Photo-induced biosynthesis of silver nanoparticles from aqueous extract of *Dunaliella salina* and their anticancer potential, J. Photochem. Photobiol., B 166 (2017) 202–211, https://doi.org/10.1016/j.jphotobiol.2016.11.020.

[36] E. Mostafavi, A. Zarepour, H. Barabadi, A. Zarrabi, L.B. Truong, D. Medina-Cruz, Antineoplastic activity of biogenic silver and gold nanoparticles to combat leukemia: beginning a new era in cancer theragnostic, Biotechnol. Rep. 34 (2022), e00714, https://doi.org/10.1016/j.btre.2022.e00714.

[37] L.B. Truong, D.M. Cruz, H. Barabadi, H. Vahidi, E. Mostafavi, Cancer therapeutics with microbial nanotechnology-based approaches, in: Handbook of Microbial Nanotechnology, 2022, pp. 17–43, https://doi.org/10.1016/B978-0-12-823426-6.00004-8.

[38] N. Talank, H. Morad, H. Barabadi, F. Mojab, S. Amidi, F. Kobarfard, E. Mostafavi, Bioengineering of green-synthesized silver nanoparticles: in vitro physicochemical, antibacterial, biofilm inhibitory, anticoagulant, and antioxidant performance, Talanta 243 (2022), 123374, https://doi.org/10.1016/j.talanta.2022.123374.

[39] A. Gupta, S. Mumtaz, C.H. Li, I. Hussain, V.M. Rotello, Combatting antibiotic-resistant bacteria using nanomaterials, Chem. Soc. Rev. 48 (2019) 415–427, https://doi.org/10.1039/C7CS00748E.

[40] J. Li, K. Rong, H. Zhao, F. Li, Z. Lu, R. Chen, Highly selective antibacterial activities of silver nanoparticles against *Bacillus subtilis*, J. Nanosci. Nanotechnol. 13 (2013) 6806–6813, https://doi.org/10.1166/jnn.2013.7781.

[41] M. Saravanan, H. Barabadi, H. Vahidi, T.J. Webster, D. Medina-Cruz, E. Mostafavi, P. Periakaruppan, Emerging theranostic silver and gold nanobiomaterials for breast cancer: present status and future prospects, Handbook on nanobiomaterials for therapeutics and diagnostic applications (2021) 439–456, https://doi.org/10.1016/B978-0-12-821013-0.00004-0.

[42] I.S. Ahmadov, A.A. Bandaliyeva, A.N. Nasibova, F.V. Hasanova, R.I. Khalilov, The synthesis of the silver nanodrugs in the medicinal plant baikal skullcap (scutellaria baicalensis georgi) and their antioxidant, antibacterial activity, Advances in Biology & Earth Sciences 2 (2020).

[43] P. Rama, P. Mariselvi, R. Sundaram, K. Muthu, Eco-friendly green synthesis of silver nanoparticles from Aegle marmelos leaf extract and their antimicrobial, antioxidant, anticancer and photocatalytic degradation activity, Heliyon 9 (2023), https://doi.org/10.1016/j.heliyon.2023.e16277.
[44] M. Morais, A.L. Teixeira, F. Dias, V. Machado, R. Medeiros, J.A.V. Prior, Cytotoxic effect of silver nanoparticles synthesized by green methods in Cancer, J. Med. Chem. 63 (2020) 14308–14335, https://doi.org/10.1021/acs.jmedchem.0c01055.
[45] A.M. Abu-Dief, L.H. Abdel-Rahman, M.A. Abd-El Sayed, M.M. Zikry, A. Nafady, Green synthesis of AgNPs ultilizing *Delonix regia* extract as anticancer and antimicrobial agents, ChemistrySelect 5 (2020) 13263–13268, https://doi.org/10.1002/slct.202003218.
[46] K. Rajendran, S. Sen, S.L. Senthil, T.V. Kumar, Evaluation of cytotoxicity of hematite nanoparticles in bacteria and human cell lines, Colloids Surf. B Biointerfaces 157 (2017) 101–109, https://doi.org/10.1016/j.colsurfb.2017.05.052.
[47] N. Gogoi, P.J. Babu, C. Mahanta, U. Bora, Green synthesis and characterization of silver nanoparticles using alcoholic flower extract of *Nyctanthes arbortristis* and in vitro investigation of their antibacterial and cytotoxic activities, Mater. Sci. Eng. C. 46 (2015) 463–469, https://doi.org/10.1016/j.msec.2014.10.069.
[48] N. Aktepe, A. Baran, Green synthesis and antimicrobial effects of silver nanoparticles by pumpkin *Cucurbita maxima* fruit fiber, Med. Sci. 11 (2022) 794–799, https://doi.org/10.5455/medscience.2022.02.036.
[49] F. Xie, P. Eric, P.J. Halley, L. Avérous, Starch-based nano-biocomposites, Prog. Polym. Sci. 38 (2013) 1590–1628, https://doi.org/10.1016/j.progpolymsci.2013.05.002.
[50] P. Cheviron, F. Gouanvé, A. Espuche, Effect of silver nanoparticles' generation routes on the morphology, oxygen, and water transport properties of starch nanocomposite films, J. Nanoparticle Res. 17 (2015) 1–16, https://doi.org/10.1007/s11051-015-3173-4.
[51] M.F. Baran, C. Keskin, A. Baran, A. Eftekhari, S. Omarova, R. Khalilov, M.N. Atalar, The investigation of the chemical composition and applicability of gold nanoparticles synthesized with *Amygdalus communis* (almond) leaf aqueous extract as antimicrobial and anticancer agents, Molecules 28 (2023) 2428, https://doi.org/10.3390/molecules28062428.